CHEMISTRY OF MATERIALS

Article

pubs.acs.org/cm

Tunable and Energetically Robust PbS Nanoplatelets for Optoelectronic Applications

Huashan Li, David Zhitomirsky, and Jeffrey C. Grossman*

Department of Materials Science and Engineering, Massachusetts Institute of Technology, Cambridge, Massachusetts 02139United States

Supporting Information

ABSTRACT: PbS nanoplatelets (NPLs) are proposed as robust materials for novel optoelectronic devices. Compared to quantum dot assemblies, ab initio simulations are employed to show that such pseudo-two-dimensional systems may provide stronger absorption and higher carrier mobility due to the distinct wave function distributions, large electronic couplings, and small hopping barriers. More importantly, both energetic and spatial traps are absent in conditions far from charge balance, indicating an extraordinary robustness against off-stoichiometry as a result of surface homogeneity and sufficient cross-linking. Based on our findings, we present several types of optoelectronic device architectures spanning photovoltaics and photodetectors that could take advantage of the superior properties found in NPLs.

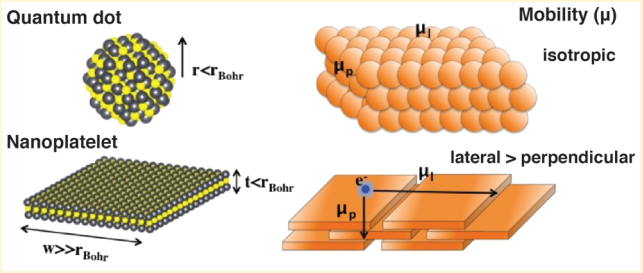

INTRODUCTION

The past few years have witnessed a rapid development of colloidal quantum dot (CQD)-based solar cells.[1−3] Further improvement of device performance, however, is currently impeded by a compromise between light absorption and charge extraction.[1,4] Since the overall absorption strength of CQDs is insensitive to both dot size and chemical environment,[5,6] increasing carrier diffusion lengths is widely accepted as a feasible way to address this dilemma.[4] With impressive carrier mobilities achieved by ligand exchange procedures, the charge diffusion length is now governed by density of recombination centers,[4] which may originate from off-stoichiometry,[7,8] surface oxidation,[9] fusion between dots,[4] and electronic impurities.[10] Despite substantial recent progress toward eliminating trap states,[11−13] the proportion of traps caused by off-stoichiometry—an intrinsic challenge of ionic compounds—is hard to avoid due to the difficulty of precise control over composition in each CQD.

Beyond the tunable bandgaps as in CQDs, nanoplatelets (NPLs) provide unique electronic and optical properties that may overcome some of the challenges in CQD-based solar cells (Figure 1). While layered solid-state compounds can be accurately produced by complicated melt-growth strategies,[14] recent advances in solution-based techniques such as orientation attachment[15,16] and cation exchange[17] enable efficient synthesis of CdSe[18−20]/CdS[18]/PbSe[17]/PbS[15−17,21] NPLs (also referred to as colloidal quantum wells), with controlled and uniform thickness achieved in CdS/CdSe NPL assemblies, which opens new opportunities to fabricate NPL-based devices. Among these pseudo-two-dimensional (pseudo-2D) systems, the case of PbS NPL is especially suitable for photovoltaic applications owing to the match between its absorption and the solar spectrum, as well as the possibility to access efficient carrier transport revealed by the reported ligand exchange with bidentate ligands[21] and lamellar mesophase.[15]

Since the development of synthesis techniques for PbS NPLs is still at its early stage, the intrinsic material properties are difficult to determine because of the relatively broad thickness distribution.[21] Nevertheless, the unique characteristics of NPLs have been demonstrated by numerous investigations on CdSe/CdS nanoplatelets, including extremely narrow emission peaks,[18,22] substantial reductions of fluorescent lifetime,[18,23] negligible Stokes shifts,[18,22] and efficient fluorescence resonance energy transfer (FRET).[19,24] In principle, the large dipole coupling and narrow energy distribution as demonstrated by the efficient FRET type energy transport[19] reveals the possibility of efficient charge transport. This has not been achieved yet due to the high density of defect states induced by ligand exchange procedures, which are necessary to obtain sufficient electron coupling.[25]

Even though the chemical properties of PbS with the rock-salt crystal structure are quite different from those of CdS/CdSe with the zinc-blende structure, PbS and CdS/CdSe NPLs are expected to share many common features as compared to their CQD counterparts. For instance, the narrow emission peaks, negligible Stokes shifts, and efficient FRET observed in CdS/CdSe NPLs, which arise from the narrow energy distribution as a consequence of the pseudo-2D quantum confinement,[18,19,22] are likely to be preserved in PbS NPLs. Additionally, the substantial reduction of fluorescent lifetime,

Received: January 14, 2016
Revised: February 20, 2016
Published: February 21, 2016

DOI: 10.1021/acs.chemmater.6b00167
Chem. Mater. 2016, 28, 1888−1896

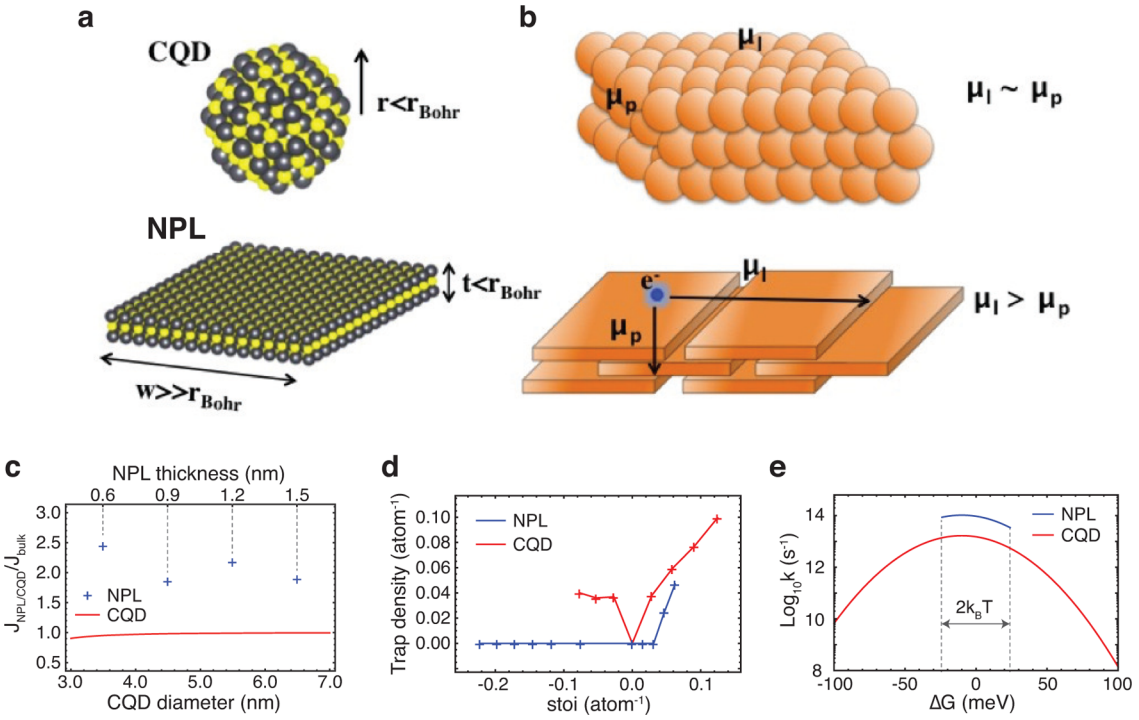

Figure 1. Properties of nanoplatelets. (a) Comparison of colloidal quantum dots (CQDs) and nanoplatelets (NPLs). In CQDs, the radius must be tuned below the exciton Bohr radius in bulk in order to achieve bandgap-size tuning. In NPLs, the lateral dimension can be of any size larger than the Bohr radius, and the thickness of the structure is used to achieve quantum tuning by adjusting the number of monolayers. (b) Schemes for making interconnected networks of CQDs and NPLs. In the CQD case, the resultant thin films are generally considered to be isotropic and hence mobility invariant given the direction. In contrast, NPLs offer different modes of carrier transport, where mobility within the sheet, μ_l, is different (and greater) than mobility between sheets μ_p. μ_l and μ_p refer to the lateral and perpendicular mobilities as drawn on the figure, respectively. Panels c–e summarize the potential advantages of PbS NPLs compared to CQDs in PV applications. (c) Enhancements of absorption flux in CQDs (J_{CQD}) and NPLs (J_{NPL}) compared to the bulk PbS (J_{bulk}). J_{CQD} were estimated by integrating over the calculated bulk PbS absorption spectrum from the optical gaps reported in experiments.[52] J_{NPL} were computed from the calculated absorption spectra of NPLs containing three to six layers. (d) Trap-state density in our prototype NPLs and CQDs with various stoichiometry per atom (stoi). For stoi < 0 the iodine atomic ligands are on the surface of the NPL while for stoi > 1 the I atoms are substitutionally doped inside the platelet. (e) Polydispersity dependent carrier hopping rates of CQDs and NPLs. The driving force ΔG correlates with the dispersion of energy levels in CQD/NPL ensembles. The electron couplings were set as 10 and 20 meV for CQD and NPL, while the reorganization energies were set as 10 meV.

originating from the large in-plane coherence area of the exciton center-of-mass motion in quasi-2D systems,[26] may also be present in PbS NPLs. On the other hand, since the surface of a PbS NPL is a {100} nonpolar surface[21] while that of CdS/CdSe NPL is a {100} polar surface,[18] their interactions with ligands and neighboring NPLs could be quite different.

In line with the scarcity of experiments, to the best of our knowledge, the only theoretical study on PbS NPLs illustrates a $1/L$ dependence of energy gap on thickness (L) using density functional theory (DFT),[21] consistent with a previous study on the quantum confinement and luminescence lifetime of PbSe NPL using tight binding calculations.[27] So far, accurate simulations that include both spin–orbit coupling and excitonic effects are lacking for predictions of optical properties of PbS NPLs. In addition, both carrier transport and trap-state properties have not been explored, which are important factors for the optimization of passivation and connectivity strategies. Furthermore, the advantages and disadvantages of PbS NPLs serving as a PV material compared to PbS CQDs have not been considered, yet such a comparison would provide important insight and possible guidelines for designing future devices.

In this work we explore the potential of PbS NPL-based solar cells using ab initio simulations and compare them with CQDs as illustrated in Figure 1a. In contrast to CQDs, NPLs are only quantum-confined in one dimension by adjusting the number of layers, enabling new packing motifs and charge transport paradigms. Our results suggest that compared to PbS CQDs, both absorption strength and carrier diffusion lengths can be improved by this quasi-2D architecture, because of the distinct wave function localization, large electronic couplings, small reorganization energies, and, more importantly, the extraordinary robustness against deleterious effects caused by off-stoichiometry. Even in highly off-stoichiometric Pb:S ratios, both energetic and spatial traps are absent in NPL assemblies due to the high surface homogeneity and appropriate connectivity. Furthermore, the processing of these colloidal materials results in vastly different configurations (Figure 1b), where CQD films are generally isotropic after ligand exchange, while films of NPLs can employ variability in the size of the lateral dimension to achieve different morphologies, and transport in the lateral dimension is expected to be improved over hopping between nanomoieties in either case.

COMPUTATIONAL METHODS

Most of our calculations were performed on infinite NPLs (quantum wells) because they appropriately represent the pseudo-2D nanoplatelets synthesized in experiments, which possess lateral dimensions (50–1000 nm[17,21]) much larger than the Bohr radius (18 nm[28]) of bulk PbS. Based on experimental observations,[21] a series of individual PbS NPLs containing 3–24 layers with their top surfaces facing the

DOI: 10.1021/acs.chemmater.6b00167
Chem. Mater. 2016, 28, 1888–1896

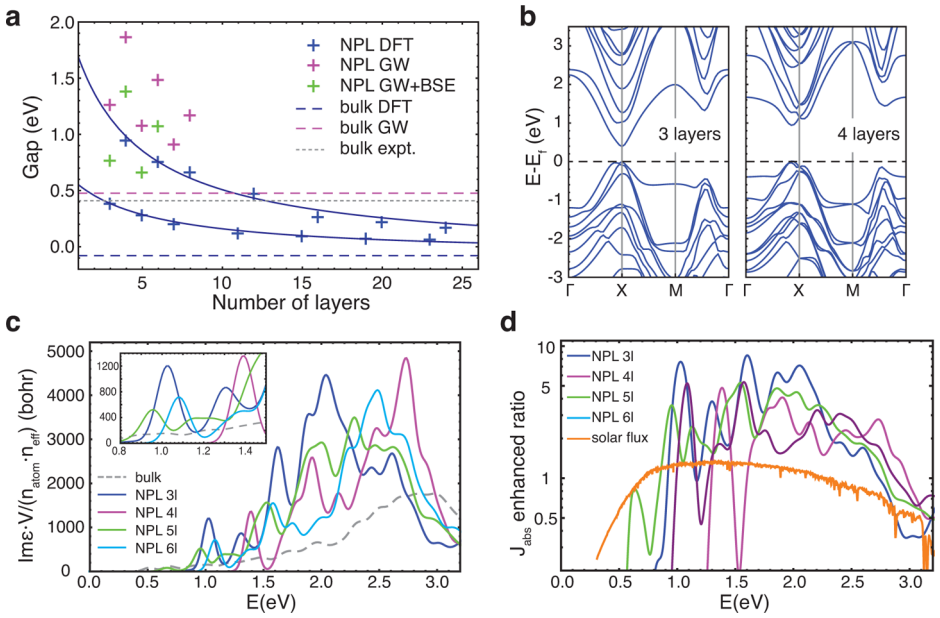

Figure 2. Electronic and optical properties of PbS NPLs. (a) Single-particle bandgaps, quasiparticle gaps, and optical gaps of NPLs with various thicknesses calculated by DFT, GW, and GW+BSE approaches, respectively. Bandgaps of bulk PbS obtained by both simulation and experiment[39] are shown for comparison. The solid curves are fitted to the DFT gaps of NPLs containing odd or even number of layers (n) with the following relation: $E_{NPL} = E_{bulk} + 1/(bn + c)$. (b) Bandstructures of PbS NPLs containing three (left) and four (right) layers, with the Fermi levels denoted by dashed lines. The k points in unit of reciprocal lattice are Γ = {0,0,0}, X = {0.5,0.0,0.0}, and M = {0.5,0.5,0.0}. (c) Absorption spectra of bulk PbS and NPLs, where Imϵ is the imaginary part of the dielectric function, n_{atom} is the number of atoms, and V and n_{eff} are the volume and effective refractive index of the simulation cell. (d) Enhancement of absorption flux (J_{abs}) in PbS NPLs compared to bulk PbS with the same thickness. The solar flux is presented in arbitrary units.

{001} orientation were used as our prototype systems. Standard DFT including spin−orbit coupling effects with the PBE[29] exchange-correlation functionals were employed to obtain the geometry, bandstructure, and charge density using the Quantum Espresso (v5.1.1) packages.[30] A one-shot GW approach with the generalized plasmon-pole model[31] was applied to determine quasiparticle levels, while the Bethe−Salpeter equation (BSE)[32] was used to compute the optical absorption spectrum with excitonic effects as implemented in the BerkeleyGW (v1.1) package.[33] For the connected PbS NPLs, the electronic structures were calculated by DFT with the projector-augmented-wave (PAW) type pseudopotentials[34] using the VASP-(v5.3)[35] package. The phonon-assisted charge hopping rates were obtained by Marcus theory,[36] which provides reasonable results when the donor and acceptor levels are similar to each other.[37,38] Further details regarding the computational methods are provided in the Supporting Information section A.

RESULTS AND DISCUSSION

Layer Dependent Quantum Confinement and Strong Absorption Flux. As illustrated in Figure 2a, our calculated quasiparticle gap by GW method of bulk PbS is 0.48 eV, in reasonable agreement with the experimental value of 0.41 eV measured at room temperature.[39] For PbS NPLs, our DFT simulations suggest that systems containing odd and even numbers of layers give two series of bandgaps roughly following a $1/L$ dependence versus thickness, with the scaling behavior consistent with previous studies.[21] While small differences of bandgaps between NPLs with odd and even numbers of layers have been reported by a theoretical study on PbSe NPLs[27] (~0.1 eV), the splitting as large as 0.5 eV observed in our calculations for PbS NPLs is surprising, which can be explained by the various degrees of quantum confinement effects originating from the symmetry dependent wave function delocalization. That is, the hybridization between Pb and S orbitals in NPLs containing odd numbers of layers are stronger than those in NPLs containing even numbers of layers (Supporting Information section B). These effects provide opportunities for establishing type-II heterojunctions between PbS even/odd NPLs, which may be of interest for PV applications.

Our more accurate GW-BSE calculations, which include many-body effects, exhibit similar trends as found in DFT, and the computed optical gaps of PbS NPLs containing three to six layers (Table 1) are consistent with PL measurements of ensembles of nanoplatelets with 1.2 ± 0.2 nm thickness (0.82 ± 0.08 eV).[21] In contrast to the strong screening effects and thus large exciton Bohr radius of 18 nm[28] in bulk PbS, for the NPLs in the thickness range suitable for PV applications (0.9−2.1 nm), the exciton radii are substantially reduced due to the strengthened Coulomb interactions (Table 1, Supporting Information section B), leading to large exciton binding energies comparable to those of polymer absorbers in organic solar cells.[40] In comparison, optimal CQD-based films for PV

Table 1. Quasiparticle HOMO/LUMO Levels calculated by GW method, Optical Gaps (E_{opt}), Exciton Binding Energies (E_b), and Exciton Sizes in the Lateral Dimension (L_{ex}) obtained by GW-BSE approach of PbS NPLs

no. of layers	HOMO (eV)	LUMO (eV)	E_{opt} (eV)	E_b (eV)	L_{ex} (nm)
3	−5.95	−4.68	0.77	0.50	1.3
4	−5.96	−4.09	1.39	0.48	1.8
5	−5.78	−4.70	0.67	0.42	1.4
6	−5.86	−4.36	1.08	0.41	2.0
7	−5.63	−4.71			
8	−5.66	−4.49			

DOI: 10.1021/acs.chemmater.6b00167
Chem. Mater. 2016, 28, 1888−1896

applications have diameters in the range of 3−5 nm, resulting in much smaller confinement and corresponding exciton binding energy (~100 meV). This indicates that unlike the spontaneous exciton dissociation in PbS CQD assemblies,[41] a type-II interface is necessary for charge separation to occur, and the PV device architecture should be designed to ensure the exciton diffusion lengths are larger than donor/acceptor domains in PbS NPL-based solar cells. In principle, this challenge may be partially addressed by alloying with other elements exhibiting larger Bohr radii such as PbSe,[22] or embedding the NPLs in environments with large dielectric constants. Both methods would need to weaken the quantum confinement while maintaining a suitable bandgap.

While in bulk PbS, the valence band maximum (VBM) and conduction band minimum (CBM) states are localized around S and Pb atoms, respectively, the broken symmetry in NPLs leads to planar VBM and CBM states that are no longer separated from each other. The corresponding enhancement of wave function overlap substantially increases the oscillator strengths of NPLs, resulting in stronger absorption compared to the bulk crystal. To quantify this effect, we compared the absorption strengths per atom of NPLs to that of bulk PbS (see Figure 2c). Unlike the gradually increasing absorption strength with increasing energy in the bulk crystal, the spectra of NPLs contain many prominent peaks with their positions depending on the NPL thickness. The amplification of absorption strength for NPLs is significant over the entire solar spectrum (Figure 2d), leading to substantial enhancement in the absorption flux compared to bulk (Table 2).

Table 2. Absorption Fluxes of PbS NPLs (J_{NPL}) Containing Three to Six Layers and Those of the Bulk Crystal with the Same Thickness (J_{bulk}), Obtained by Integrating over the Product of Absorbance and Solar Spectrum

no. of layers	J_{NPL} (mA·cm^{-2})	J_{bulk} (mA·cm^{-2})
3	0.79	0.32
4	0.80	0.43
5	1.17	0.54
6	1.22	0.64

By contrast, because of their similar wave function distributions, the absorption strengths of PbS CQDs are expected to be similar to those of bulk PbS except for the range near the band edge, as verified experimentally.[5] As GW-BSE simulations are computationally too demanding for CQDs, the random phase approximation (RPA) was instead applied to probe qualitatively CQDs with various sizes and shapes. The results suggest that for the small CQDs (d = 1.2−2.1 nm) considered in this work, the absorption spectrum is quite sensitive to the shape of the dot, while the absorption strength generally increases with increasing dot size, and eventually approaches that of the bulk crystal. This can be explained by the fact that the wave function distributions at the CQD surface are less favorable for overlap between occupied and unoccupied orbitals compared to those inside the bulk crystal. In all cases, the absorption strengths of PbS CQDs are much lower than those of NPLs (Supporting Information section C).

Extraordinary Robustness against Off-Stoichiometry. In parallel to improving absorption efficiency, eliminating trap states is another important way to further enhance the device efficiency, which remains a challenge so far because the origin of trap states is not fully understood, and both the type and density of trap states exhibit strong dependence on CQD size,[42] component,[43] and surface passivation.[44] Generally, they can arise from off-stoichiometry,[7,8] electronically active impurities,[10] formation of Pb dimers,[45] surface oxidation,[9] fusion and aggregation,[4,46] and interfacial dipole moment.[46] While most of the basic traps associated with the overall characteristics of a CQD ensemble are possible to address by appropriate ligands and advanced synthesis techniques, as suggested by the substantial reduction of midgap-state density in recent experiments,[9,11,13] eliminating off-stoichiometry related trap states is much more difficult as the electronic structure is sensitive to stoichiometry,[7,8] and meeting the charge balance criterion requires a precise control over the proportion of components in each CQD. In this sense, designing strategies to reduce the deleterious impacts of off-stoichiometry is critical for future colloidal CQD-/NPL-based devices.

We found that PbS NPLs can provide extraordinary robustness against off-stoichiometry compared to PbS CQDs. By tuning the degree of passivation, the off-stoichiometry can be negative or positive. Our results suggest that such advantage of PbS NPLs originates from their intrinsic structural benefits: (1) as the Pb:S ratio in pristine NPLs is exactly 1:1, the presence of ligands shifts the off-stoichiometry from zero to negative, which eliminates a large proportion of energetic traps by reducing the density of aggregated Pb atoms that are more likely to form in positive off-stoichiometric conditions; (2) the homogeneity of the {001} surface, absence of {111}/{011} facets, and resulting lack of intersections between different facets in NPLs provide another degree of protection against spatial trap states as the relevant microstructures become more difficult to generate; (3) the planar surface and lamellar stacking architecture enables sufficient cross-linking between NPLs, which prevents aggregation of ligands.

In general, trap states induced by off-stoichiometry in ionic compounds have detrimental effects on carrier transport that can be classified into two types: energetic traps (midgap states) that increase hopping barriers and spatial traps (states with localized wave functions) that reduce electron couplings. As examples, we examined both types for I passivated 2.2 nm PbS CQDs and NPLs containing four layers (Figure 3). Iodide was chosen as the prototypical ligand due to its importance for processing of PbS CQD films with optimal optoelectronic properties[47,48] and inherent experimental compatibility with the proposed nanoplatelet structures. Additionally, it offers a fine degree of control over the stoichiometry and, due to being sterically small, enables exploration of a wide parameter space.

The Pb-rich CQDs were generated by the Wulff construction with various surface coverages and a random distribution of ligands. Consistent with previous studies,[8] only shallow energetic traps exist with a negative off-stoichiometry, while many deep trap states arise with a positive off-stoichiometry (Figure 3a). For the stoichiometric CQD, the bandgap is clean (no traps), and the wave functions are delocalized over the entire dot. When the off-stoichiometry is positive, the deep energy traps also appear to be spatial traps (Figure 3c), mainly localized at the intersections of different facets, and around the structures of Pb atoms bridged by an I atom or Pb dimer/trimer. When the off-stoichiometry is negative, the shallow energetic trap states may serve as spatial traps mainly localized near Pb atoms that deviate from regular sites at the {001} facet or aggregations of I atoms (Figure 3d).

For PbS NPLs with I atoms on their surfaces, the electronic structures are not sensitive to the passivation sites, and neither

DOI: 10.1021/acs.chemmater.6b00167
Chem. Mater. 2016, 28, 1888−1896

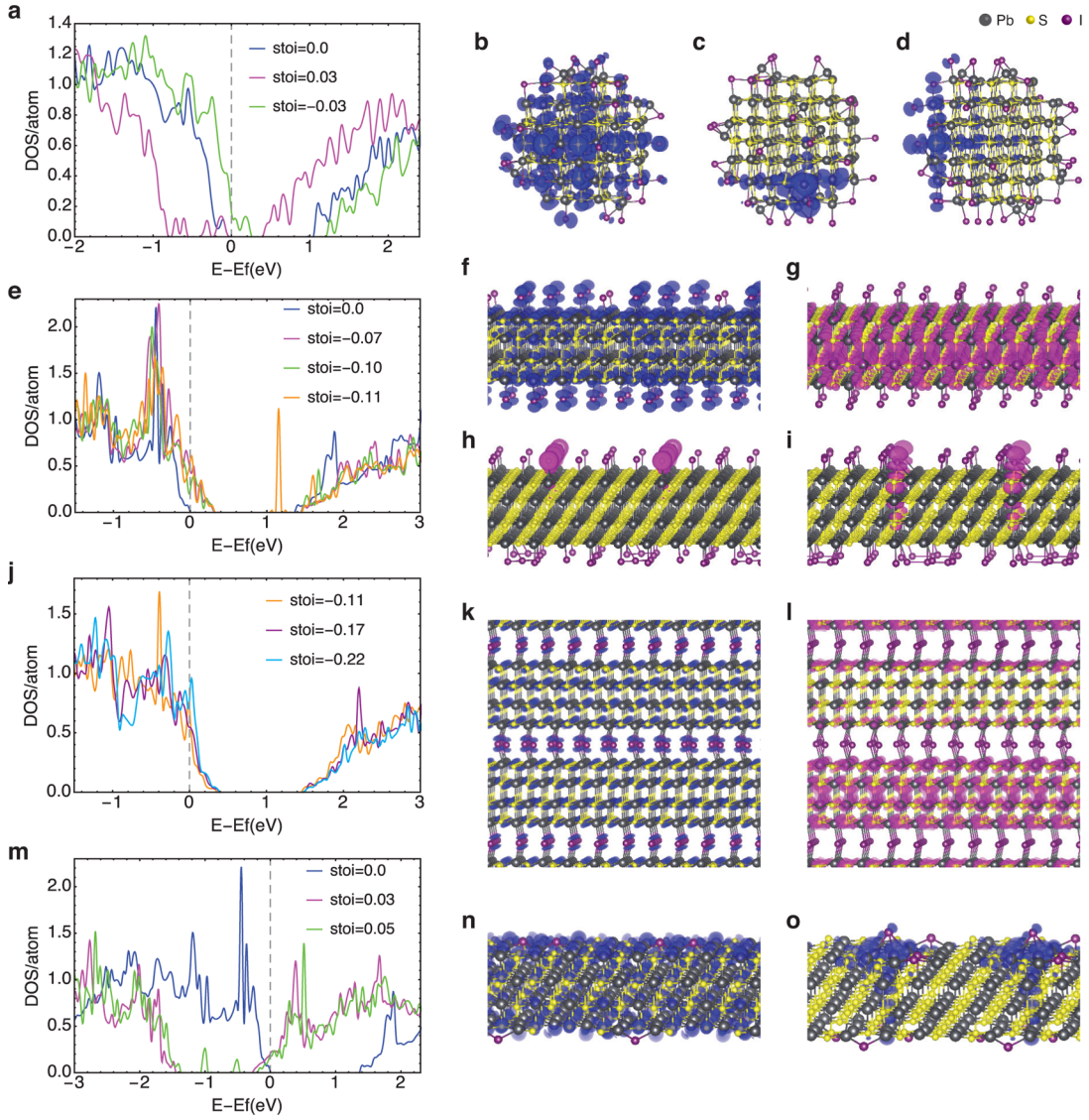

Figure 3. Robustness against off-stoichiometry of PbS NPLs compared to QDs. (a) Density of states (DOS) of PbS QDs with various stoichiometries. The term "stoi" denotes stoichiometry/atom, and the dashed lines present the Fermi levels. (b) Wave functions of orbitals near the valence band edges of (b) $Pb_{135}S_{116}I_{38}$ (stoi =0.0), (c) $Pb_{135}S_{116}I_{30}$ (stoi = 0.03), and (d) $Pb_{135}S_{116}I_{46}$ (stoi = −0.03). (e) DOS of isolated PbS NPLs with various stoichiometry. Wave functions of orbitals near the (f) valence and (g) conduction band edges of $Pb_{64}S_{64}I_{10}$ (stoi = −0.07). Wave functions of orbitals near the conduction band edges of (h) $Pb_{64}S_{64}I_{14}$ (stoi = −0.10) and (i) $Pb_{64}S_{64}I_{16}$ (stoi = −0.11). (j) DOS of stacking PbS NPL arrays with various stoichiometry. Wave functions of orbitals near the (k) valence and (l) conduction band edges of $Pb_{128}S_{128}I_{32}$ (stoi = −0.22). (m) DOS of PbS NPLs with substitution defects and various stoichiometry. Wave functions of orbitals near the conduction band edges of (n) $Pb_{64}S_{60}I_4$ (stoi = 0.03) and (o) $Pb_{64}S_{60}I_6$ (stoi = 0.05).

energetic (Figure 3e) nor spatial traps (Figure 3f,g) are observed with off-stoichiometry up to −0.07/atom, in contrast to the appearance of spatial traps in CQDs with off-stoichiometry = −0.03/atom (Figures 3d). Further increase of the off-stoichiometry in NPLs first produces spatial traps while preserving a clean bandgap, which is ascribed to the chemical bonding between I atoms at high ligand density (Figure 3h). Once the off-stoichiometry approaches −0.11/atom (50% of the surface Pb atoms are passivated), midgap states appear as a consequence of the formation of Pb−I−S structures (Figure 3i). Such trap states can be eliminated by employing a lamellar stacking architecture as shown in Figure 3j. As the I atoms between NPLs prefer to bond with Pb atoms, both I−I and I−S bonds are absent even at very high ligand densities. As a consequence, both energetic (Figure 3j) and spatial (Figures 3k,l) traps are absent with off-stoichiometry up to −0.22/atom (full coverage of the surface) for this architecture.

Even though most organic ligands will not be able to penetrate into PbS NPLs, for the case of atomic ligands a small amount could substitute for the S atoms inside NPLs,[7] resulting in a positive stoichiometry. According to our calculations, for this case, while nontrivial distortions would be induced by I substitutions, the clean bandgaps are preserved (Figure 3m) and the wave functions remain delocalized over the entire NPL (Figure 3n) with off-stoichiometry up to 0.03/atom. However, both energetic and spatial trap states appear if the off-stoichiometry is further increased, which we can attribute to the formation of Pb−Pb bonds at higher doping densities (Figure 3o). More details regarding the PDOS and wave

DOI: 10.1021/acs.chemmater.6b00167
Chem. Mater. 2016, 28, 1888−1896

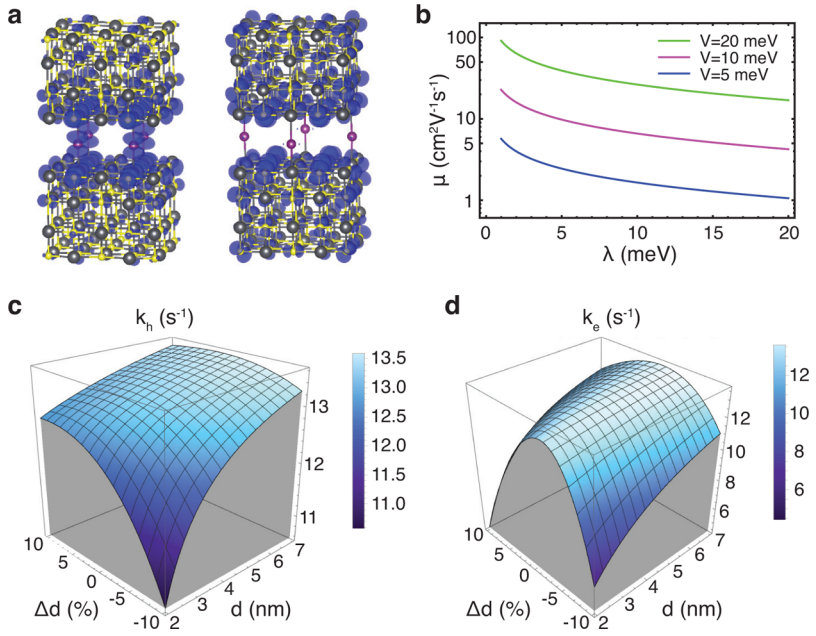

Figure 4. Comparison of transport properties between PbS NPLs and QDs. (a) HOMO wave functions of nanoplatelet dimer with 4 I bridges in the middle (left) and at the edge (right) of the interface. (b) Carrier mobilities of stacking NPL assemblies given various electron couplings (V) and reorganization energies (λ). (c) Hole and (d) electron hopping rates between two QDs with diameter d and $d + \Delta d$.

functions for off-stoichiometric PbS NPLs and CQDs are provided in Supporting Information section D.

In realistic NPLs, the existence of partial layers could have the potential to produce new types of trap states compared to CQDs. In order to test the robustness of electronic structure against imperfections, we studied the cases of PbS NPLs containing four layers with various partial layers. Since the gaps of NPLs containing three and five layers are smaller than that with four layers, both concave and convex sites reduce the bandgap as expected. However, the variations of the bandgap are relatively minor, and neither energetic nor spatial traps are present in any case, indicating that the NPL electronic structure is quite robust to such imperfections (Supporting Information section E).

Efficient Phonon-Assisted Carrier Transport. In addition to the need for a clean (i.e., trap-free) bandgap, efficient carrier transport is crucial to device performance. According to the Marcus equation,[36] this can be achieved by reducing the driving forces (energy broadening) and reorganization energy that lead to a small effective hopping barrier or by enhancing the electron couplings via appropriate connectivities. To this end, we considered the cases of bridging NPLs by I atoms and by necking (fusing).

We have seen that the reductions of bandgaps for prototype four-layer NPL assemblies with both types of connectivity compared to that of an isolated NPL are substantial (Figure 3e), implying that the electron couplings between neighboring NPLs are strong even with a low density of connections. To qualitatively estimate the electron coupling relevant to the highest connectivity density that avoids trap states, we introduce auxiliary systems of finite platelet dimers with the same densities of connectivity. Such an approximation is justified since the key factors that determine electron coupling within the superexchange scenario (electronic overlap between the dots increased by covalent bonds between the dots and the bridge), the wave function overlap and energy level offset, are similar for the original and auxiliary systems. The computed electron coupling for hole transport with bridging and necking are 111 and 25 meV, respectively, while those for electron transport are 22 and 41 meV. This indicates bridging by I atoms is more favorable for p-type while necking is more favorable for n-type transport. Reducing the density of I bridges by half gives a coupling of 63 meV for hole transport, which is nearly half of the original value (111 meV), implying that bridge-assisted superexchange is the dominant coupling mechanism between occupied orbitals. In the meantime, the reduction of coupling from 25 to 20 meV for electron transport is much less significant, implying that direct coupling between delocalized wave functions enabled by the short distance between platelets may play an important role in coupling between unoccupied orbitals.

In order to understand the influence of boundaries, we moved the connectivities to the edge and corner sites of the platelets, leading to a decrease in electron coupling for the case of necking, and even more dramatic reductions of coupling and introduction of additional trap states in the case of bridging (Figure 4a). Additionally, the impact of donor/acceptor shape on electron coupling was explored by modifying the thickness of the platelets. As expected, the coupling drops with increasing thickness due to inefficient wave function overlap (Supporting Information section F). From this discussion, we can understand why the electron coupling between PbS CQDs is much weaker than that between NPLs, namely, because of the smaller surface area for connectivity and larger distance between donor and acceptor wave functions, consistent with the small electron couplings (<10 meV) between PbS CQDs obtained in previous simulations.[46]

Another attractive characteristic of NPLs is their tunable reorganization energy. Following the scaling analysis of electron−phonon coupling effects in previous theoretical studies,[37] the reorganization energy of a sufficiently large platelet scales as $\lambda \propto d^{-2}$, where d is the diameter of the delocalized wave function. For our prototype systems of nanoplatelets containing four layers, while the lateral sizes are

DOI: 10.1021/acs.chemmater.6b00167
Chem. Mater. 2016, 28, 1888−1896

not large enough for fitting or extrapolation, λ tends to decrease with increasing size, and the largest sample with $d \approx 2$ nm gives an upper bound (hole, 19 meV; electron, 37 meV) of reorganization energies (Supporting Information section G). This means that, by increasing the platelet size and homogeneity, the reorganization energies can be reduced to values that are much smaller than the electron couplings, which may result in a transition of transport mechanism from phonon-assisted hopping to coherent band transport associated with a much higher mobility.

In addition to the intrinsic advantages of larger electron coupling and smaller reorganization energy compared to CQDs, the improved robustness of the ensemble energy profile against size dispersion makes NPLs favorable for carrier transport. Specifically, the quantum confinement effects in a NPL rely only on its thickness, and thus the dispersity of lateral size will not contribute to the energy distribution. To illustrate the potential benefits, we considered assemblies of NPLs containing four layers in the zero-polydispersity limit, wherein the driving force of carrier hopping is zero if thermal fluctuations are neglected. Our results show that, with appropriate lateral size and connectivity, the carrier mobility has the potential to reach a value of ~10 $cm^2\ V^{-1}\ s^{-1}$ (Figure 4b). The current limitations in experiments that prevent us from accessing such a high mobility are thickness distribution and defects induced by the ligand exchange procedure, which may have a noticeable impact on both hopping barriers and electron couplings. We note that, in any case, charge hopping between neighboring platelets will be much less efficient than the band-like transport along the lateral direction inside a platelet (the carrier mobility of bulk PbS is 500−700 $cm^2\ V^{-1}\ s^{-1}$[149]), implying that sufficiently small devices should include only lateral transport within the platelets. For PV applications, though, pure hopping in the normal direction of a lamellar architecture may be more favorable than a mixture of normal and lateral transport, because the wave function overlap and thus the electron coupling, can be dramatically reduced in other architectures.

In contrast, polydispersity in defect-free CQD assemblies is harmful to device performance when the corresponding energy broadening is greater than 50 meV.[50,51] Using the experimental values for the HOMO and LUMO energy levels of PbS CQDs,[52] we find that, for typical values of size dispersion (~10%),[51] the associated eigenvalue deviations in small dots (3−7 nm) could be as large as 100 meV (Supporting Information section H). With reorganization energies extrapolated from the values of a 2.1 nm CQD and electron coupling of 10 meV (an upper bound from previous calculations), the carrier hopping rates between two CQDs as a function of dot-size deviation were estimated by Marcus theory and shown in Figure 4c,d. Since the LUMO level has a stronger dependence on dot size than the HOMO level, and the effective hopping barrier is related to both the driving force and reorganization energy, the size deviation has different impacts on the electron and hole hopping rates. Regarding the hole transport, the size difference increases the hopping rate from one dot to the other while blocking the reverse process, leading to hole trapping in the larger dot. For the electron transport, the large driving force caused by size difference results in a several orders of magnitude reduction of the hopping rate in both directions. This indicates that the energy broadening originating from 3D quantum confinement serves as a challenge to further improve the carrier mobility in defect-free CQDs.

We emphasize that the above discussion on carrier transport relies on the assumption of zero thickness variation in PbS NPLs, which is achievable due to the area independent energy levels in such pseudo-2D systems, and necessary for achieving high-performance devices because of the large difference of bandgaps between NPLs with different numbers of layers. This indicates that advanced experimental techniques are required although we note that the CdSe/CdS NPLs with well-defined thicknesses have already been successfully synthesized.[18−20]

Insights for NPL-Based Photovoltaics and Photodetection Devices. While a range of electronic and optical properties of PbS NPLs have been investigated in this study, the prediction of solar cell performance and other optoelectronic devices requires analysis of charge dynamics determined by competing procedures including energy transfer, photoluminescence, charge transfer, polaron dissociation, nonradiative recombination, and carrier transport, etc., as well as more sophisticated designs of device architecture, which are beyond the scope of this work. We instead offer a few insights into novel types of devices that may be constructed with PbS NPLs that leverage the size tunability into the infrared with degrees of freedom that have not been previously available with CQDs. Figure 5a represents a typical donor/acceptor type photovoltaic device, where in the case of NPLs, such donor and acceptor materials would be able to be constructed all within the same materials system by tuning the thickness of each type of NPL. Given the high exciton binding energies, however, these materials would need to transport excitons efficiently to the charge-separating interface; the prospect of sub-monolayer insensitivity in electronic properties in these materials presents an opportunity to make films that are polydispersity-resistant, hence allowing for efficient energy transfer. Conversely, if rapid carrier separation is required, excitons may be split by using a bulk-heterojunction type architecture (Figure 5b). Here, the NPLs are aligned in a way that interlaces the donor and acceptor phases, thus making a ubiquitous charge-separating interface throughout the device. The complexity of forming such an architecture may be overcome by using such methods as electrophoretic deposition, where the NPLs may align in response to the applied electric field and result in perpendicular orientation as they deposit on the electrodes. Importantly, the lateral mobility within the NPL is expected to be higher than

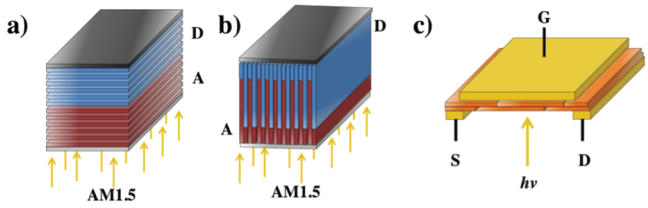

Figure 5. Optoelectronics based on nanoplatelets. (a) Layered sheets of nanoplatelet (NPLs) in a donor/acceptor fashion may enable charge separation and extraction, providing sufficient exciton transport lengths and efficient charge separation at the junction. Different thickness NPLs may be used to establish the heterojunction offsets. (b) Bulk heterojunciton concept that enables rapid exciton dissociation and charge extraction by interpenetrating different thickness NPLs to establish the heterojunction. (c) Concept for a thin film phototransistor (with additional gate for better ON/OFF characteristics). This type of architecture, as well as others, can enable improved light sensing in the infrared leveraging high lateral mobility and quantum tuned NPLs.

DOI: 10.1021/acs.chemmater.6b00167
Chem. Mater. 2016, 28, 1888−1896

hopping between NPLs (or between CQDs), allowing efficient charge transport to the electrodes. Finally, NPLs tuned in the infrared can be utilized for photodetection, with one type of scheme shown in Figure 5c, again benefiting from the high lateral mobility and improved absorption over more conventional nanomaterials such as CQDs. NPLs present an opportunity to re-engineer current nanomaterials-based devices due to their improved polydispersity insensitivity, greater absorption properties, and potential to achieve high lateral mobilities.

CONCLUSIONS

In conclusion, ab initio simulations were employed to probe the differences in electronic and optical characteristics between PbS NPLs and CQDs. The results suggest that the broken symmetry in NPLs leads to planar wave functions and parity-dependent quantum confinement effects, as well as much higher absorption strengths compared to CQDs. In addition, while energetic and spatial traps seem to be unavoidable even in slightly off-stoichiometric CQDs, both types of traps are absent in NPLs far away from the charge balance condition because of the negative off-stoichiometry, high surface homogeneity, and efficient cross-linking. Moreover, large electronic couplings and small reorganization energies may be attained in NPLs by appropriate connectivity and lateral size control, which along with the small energy broadening may give much higher carrier mobility than CQDs. Such potential improvements in absorption efficiency and diffusion length highlight the possibility to modify system properties by changing the dimensionality of nanostructures and opens an opportunity to develop novel optoelectronic devices based on NPLs.

ASSOCIATED CONTENT

Supporting Information

The Supporting Information is available free of charge on the ACS Publications website at DOI: 10.1021/acs.chemmater.6b00167.

Computational methods, electronic structures of NPLs, absorption spectrum of CQDs, analysis of trap states in off-stoichiometric NPLs/CQDs, electron coupling between platelets, size dependent reorganization energy, impact of polydispersity on charge transfer, and electronic structure of NPLs with partial layers (PDF)

AUTHOR INFORMATION

Corresponding Author

*E-mail: jcg@mit.edu.

Notes

The authors declare no competing financial interest.

ACKNOWLEDGMENTS

We are grateful to the Samsung Advanced Institute of Technology for financial support. D.Z. acknowledges his NSERC Canada Banting Postdoctoral Fellowship award. This research used resources of the National Energy Research Scientific Computing Center, a DOE Office of Science User Facility supported by the Office of Science of the U.S. Department of Energy under Contract No. DE-AC02-05CH11231. This work used the Extreme Science and Engineering Discovery Environment (XSEDE), which is supported by National Science Foundation Grant No. ACI-1053575.

REFERENCES

(1) Lan, X.; Masala, S.; Sargent, E. H. Charge-Extraction Strategies for Colloidal Quantum Dot Photovoltaics. *Nat. Mater.* **2014**, *13*, 233−240.

(2) Sargent, E. H. Colloidal Quantum Dot Solar Cells. *Nat. Photonics* **2012**, *6*, 133−135.

(3) Chen, T.; Reich, K. V.; Kramer, N. J.; Fu, H.; Kortshagen, U. R.; Shklovskii, B. I. Metal-Insulator Transition in Films of Doped Semiconductor Nanocrystals. *Nat. Mater.* **2015**, *15*, 299−303.

(4) Zhitomirsky, D.; Voznyy, O.; Levina, L.; Hoogland, S.; Kemp, K. W.; Ip, A. H.; Thon, S. M.; Sargent, E. H. Engineering Colloidal Quantum Dot Solids within and beyond the Mobility-Invariant Regime. *Nat. Commun.* **2014**, *5*, 3803.

(5) Moreels, I.; Lambert, K.; Smeets, D.; De Muynck, D.; Nollet, T.; Martins, J. C.; Vanhaecke, F.; Vantomme, A.; Delerue, C.; Allan, G.; Hens, Z. Size-Dependent Optical Properties of Colloidal PbS Quantum Dots. *ACS Nano* **2009**, *3*, 3023−3030.

(6) Leatherdale, C.; Woo, W.-K.; Mikulec, F.; Bawendi, M. On the Absorption Cross Section of CdSe Nanocrystal Quantum Dots. *J. Phys. Chem. B* **2002**, *106*, 7619−7622.

(7) Voznyy, O.; Zhitomirsky, D.; Stadler, P.; Ning, Z.; Hoogland, S.; Sargent, E. H. A Charge-Orbital Balance Picture of Doping in Colloidal Quantum Dot Solids. *ACS Nano* **2012**, *6*, 8448−8455.

(8) Kim, D.; Kim, D.-H.; Lee, J.-H.; Grossman, J. C. Impact of Stoichiometry on the Electronic Structure of PbS Quantum Dots. *Phys. Rev. Lett.* **2013**, *110*, 196802.

(9) Zhang, Y.; Zherebetskyy, D.; Bronstein, N. D.; Barja, S.; Lichtenstein, L.; Alivisatos, A. P.; Wang, L.-W.; Salmeron, M. Molecular Oxygen Induced In-Gap States in PbS Quantum Dots. *ACS Nano* **2015**, *9*, 10445−10452.

(10) Carey, G. H.; Kramer, I. J.; Kanjanaboos, P.; Moreno-Bautista, G.; Voznyy, O.; Rollny, L.; Tang, J. A.; Hoogland, S.; Sargent, E. H. Electronically Active Impurities in Colloidal Quantum Dot Solids. *ACS Nano* **2014**, *8*, 11763−11769.

(11) Hwang, G. W.; Kim, D.; Cordero, J. M.; Wilson, M. W.; Chuang, C.-H. M.; Grossman, J. C.; Bawendi, M. G. Identifying and Eliminating Emissive Sub-Bandgap States in Thin Films of PbS Nanocrystals. *Adv. Mater.* **2015**, *27*, 4481−4486.

(12) Chuang, C.-H. M.; Maurano, A.; Brandt, R. E.; Hwang, G. W.; Jean, J.; Buonassisi, T.; Bulovic, V.; Bawendi, M. G. Open-Circuit Voltage Deficit, Radiative Sub-Bandgap States, and Prospects in Quantum Dot Solar Cells. *Nano Lett.* **2015**, *15*, 3286−3294.

(13) Zhang, Y.; Zherebetskyy, D.; Bronstein, N. D.; Barja, S.; Lichtenstein, L.; Schuppisser, D.; Wang, L.-W.; Alivisatos, A. P.; Salmeron, M. Charge Percolation Pathways Guided by Defects in Quantum Dot Solids. *Nano Lett.* **2015**, *15*, 3249−3253.

(14) Segawa, K.; Taskin, A.; Ando, Y. Pb 5 Bi 24 Se 41: A New Member of the Homologous Series Forming Topological Insulator Heterostructures. *J. Solid State Chem.* **2015**, *221*, 196−201.

(15) Wang, F.; Wang, Y.; Liu, Y.-H.; Morrison, P. J.; Loomis, R. A.; Buhro, W. E. Two-Dimensional Semiconductor Nanocrystals: Properties, Templated Formation, and Magic-Size Nanocluster Intermediates. *Acc. Chem. Res.* **2015**, *48*, 13−21.

(16) Bouet, C.; Tessier, M. D.; Ithurria, S.; Mahler, B.; Nadal, B.; Dubertret, B. Flat Colloidal Semiconductor Nanoplatelets. *Chem. Mater.* **2013**, *25*, 1262−1271.

(17) Bouet, C.; Laufer, D.; Mahler, B.; Nadal, B.; Heuclin, H.; Pedetti, S.; Patriarche, G.; Dubertret, B. Synthesis of Zinc and Lead Chalcogenide Core and Core/Shell Nanoplatelets Using Sequential Cation Exchange Reactions. *Chem. Mater.* **2014**, *26*, 3002−3008.

(18) Ithurria, S.; Tessier, M.; Mahler, B.; Lobo, R.; Dubertret, B.; Efros, A. L. Colloidal Nanoplatelets with Two-Dimensional Electronic Structure. *Nat. Mater.* **2011**, *10*, 936−941.

(19) Rowland, C. E.; Fedin, I.; Zhang, H.; Gray, S. K.; Govorov, A. O.; Talapin, D. V.; Schaller, R. D. Picosecond Energy Transfer and Multiexciton Transfer Outpaces Auger Recombination in Binary CdSe Nanoplatelet Solids. *Nat. Mater.* **2015**, *14*, 484−489.

(20) Grim, J. Q.; Christodoulou, S.; Di Stasio, F.; Krahne, R.; Cingolani, R.; Manna, L.; Moreels, I. Continuous-Wave Biexciton

DOI: 10.1021/acs.chemmater.6b00167
Chem. Mater. 2016, 28, 1888−1896

Lasing at Room Temperature Using Solution-Processed Quantum Wells. *Nat. Nanotechnol.* **2014**, *9*, 891−895.
(21) Bhandari, G. B.; Subedi, K.; He, Y.; Jiang, Z.; Leopold, M.; Reilly, N.; Lu, H. P.; Zayak, A. T.; Sun, L. Thickness-Controlled Synthesis of Colloidal PbS Nanosheets and Their Thickness-Dependent Energy Gaps. *Chem. Mater.* **2014**, *26*, 5433−5436.
(22) Fan, F.; Kanjanaboos, P.; Saravanapavanantham, M.; Beauregard, E.; Ingram, G.; Yassitepe, E.; Adachi, M. M.; Voznyy, O.; Johnston, A. K.; Walters, G.; Kim, G.-H.; Lu, Z.-H.; Sargent, E. H. Colloidal $CdSe_{1-x}$ S_x Nanoplatelets with Narrow and Continuously-Tunable Electroluminescence. *Nano Lett.* **2015**, *15*, 4611−4615.
(23) Kunneman, L. T.; Schins, J. M.; Pedetti, S.; Heuclin, H.; Grozema, F. C.; Houtepen, A. J.; Dubertret, B.; Siebbeles, L. D. Nature and Decay Pathways of Photoexcited States in CdSe and CdSe/CdS Nanoplatelets. *Nano Lett.* **2014**, *14*, 7039−7045.
(24) Guzelturk, B.; Erdem, O.; Olutas, M.; Kelestemur, Y.; Demir, H. V. Stacking in Colloidal Nanoplatelets: Tuning Excitonic Properties. *ACS Nano* **2014**, *8*, 12524−12533.
(25) Lhuillier, E.; Pedetti, S.; Ithurria, S.; Heuclin, H.; Nadal, B.; Robin, A.; Patriarche, G.; Lequeux, N.; Dubertret, B. Electrolyte-Gated Field Effect Transistor to Probe the Surface Defects and Morphology in Films of Thick CdSe Colloidal Nanoplatelets. *ACS Nano* **2014**, *8*, 3813−3820.
(26) Naeem, A.; Masia, F.; Christodoulou, S.; Moreels, I.; Borri, P.; Langbein, W. Giant Exciton Oscillator Strength and Radiatively Limited Dephasing in Two-Dimensional Platelets. *Phys. Rev. B: Condens. Matter Mater. Phys.* **2015**, *91*, 121302.
(27) Allan, G.; Delerue, C. Confinement Effects in PbSe Quantum Wells and Nanocrystals. *Phys. Rev. B: Condens. Matter Mater. Phys.* **2004**, *70*, 245321.
(28) Ma, W.; Luther, J. M.; Zheng, H.; Wu, Y.; Alivisatos, A. P. Photovoltaic Devices Employing Ternary PbS x Se1-x Nanocrystals. *Nano Lett.* **2009**, *9*, 1699−1703.
(29) Perdew, J. P.; Burke, K.; Ernzerhof, M. Generalized Gradient Approximation Made Simple. *Phys. Rev. Lett.* **1996**, *77*, 3865.
(30) Giannozzi, P.; Baroni, S.; Bonini, N.; Calandra, M.; Car, R.; Cavazzoni, C.; Ceresoli, D.; Chiarotti, G. L.; Cococcioni, M.; Dabo, I.; et al. QUANTUM ESPRESSO: a Modular and Open-Source Software Project for Quantum Simulations of Materials. *J. Phys.: Condens. Matter* **2009**, *21*, 395502.
(31) Hybertsen, M. S.; Louie, S. G. Electron Correlation in Semiconductors and Insulators: Band Gaps and Quasiparticle Energies. *Phys. Rev. B: Condens. Matter Mater. Phys.* **1986**, *34*, 5390−5413.
(32) Rohlfing, M.; Louie, S. G. Electron-Hole Excitations and Optical Spectra from First Principles. *Phys. Rev. B: Condens. Matter Mater. Phys.* **2000**, *62*, 4927−4944.
(33) Deslippe, J.; Samsonidze, G.; Strubbe, D. A.; Jain, M.; Cohen, M. L.; Louie, S. G. BerkeleyGW: A Massively Parallel Computer Package for the Calculation of the Quasiparticle and Optical Properties of Materials and Nanostructures. *Comput. Phys. Commun.* **2012**, *183*, 1269−1289.
(34) Blöchl, P. E. Projector Augmented-wave Method. *Phys. Rev. B: Condens. Matter Mater. Phys.* **1994**, *50*, 17953.
(35) Kresse, G.; Furthmüller, J. Efficient Iterative Schemes for Ab Initio Total-energy Calculations Using a Plane-wave Basis Set. *Phys. Rev. B: Condens. Matter Mater. Phys.* **1996**, *54*, 11169.
(36) Marcus, R. A. Electron, Proton and Related Transfers. *Faraday Discuss. Chem. Soc.* **1982**, *74*, 7−15.
(37) Chu, I.-H.; Radulaski, M.; Vukmirovic, N.; Cheng, H.-P.; Wang, L.-W. Charge Transport in a Quantum Dot Supercrystal. *J. Phys. Chem. C* **2011**, *115*, 21409−21415.
(38) Li, H.; Wu, Z.; Lusk, M. T. Dangling Bond Defects: The Critical Roadblock to Efficient Photoconversion in Hybrid Quantum Dot Solar Cells. *J. Phys. Chem. C* **2014**, *118*, 46−53.
(39) Hummer, K.; Grüneis, A.; Kresse, G. Structural and Electronic Properties of Lead Chalcogenides from First Principles. *Phys. Rev. B: Condens. Matter Mater. Phys.* **2007**, *75*, 195211.
(40) Koster, L. J. A.; Mihailetchi, V. D.; Blom, P. W. M. Ultimate Efficiency of Polymer/Fullerene Bulk Heterojunction Solar Cells. *Appl. Phys. Lett.* **2006**, *88*, 093511.
(41) Choi, J. J.; Luria, J.; Hyun, B.-R.; Bartnik, A. C.; Sun, L.; Lim, Y.-F.; Marohn, J. A.; Wise, F. W.; Hanrath, T. Photogenerated Exciton Dissociation in Highly Coupled Lead Salt Nanocrystal Assemblies. *Nano Lett.* **2010**, *10*, 1805−1811.
(42) Bozyigit, D.; Lin, W. M. M.; Yazdani, N.; Yarema, O.; Wood, V. A Quantitative Model for Charge Carrier Transport, Trapping and Recombination in Nanocrystal-Based Solar Cells. *Nat. Commun.* **2015**, *6*, 6180.
(43) Katsiev, K.; Ip, A. H.; Fischer, A.; Tanabe, I.; Zhang, X.; Kirmani, A. R.; Voznyy, O.; Rollny, L. R.; Chou, K. W.; Thon, S. M.; et al. The Complete In-Gap Electronic Structure of Colloidal Quantum Dot Solids and Its Correlation with Electronic Transport and Photovoltaic Performance. *Adv. Mater.* **2014**, *26*, 937−942.
(44) Bakulin, A. A.; Neutzner, S.; Bakker, H. J.; Ottaviani, L.; Barakel, D.; Chen, Z. Charge Trapping Dynamics in PbS Colloidal Quantum Dot Photovoltaic Devices. *ACS Nano* **2013**, *7*, 8771−8779.
(45) Voznyy, O.; Thon, S.; Ip, A.; Sargent, E. Dynamic Trap Formation and Elimination in Colloidal Quantum Dots. *J. Phys. Chem. Lett.* **2013**, *4*, 987−992.
(46) Li, H.; Zhitomirsky, D.; Dave, S.; Grossman, J. C. Towards the Ultimate Limit of Connectivity in Quantum Dots with High Mobility and Clean Gaps. *ACS Nano* **2016**, *10*, 606.
(47) Zhitomirsky, D.; Furukawa, M.; Tang, J.; Stadler, P.; Hoogland, S.; Voznyy, O.; Liu, H.; Sargent, E. H. N-Type Colloidal-Quantum-Dot Solids for Photovoltaics. *Adv. Mater.* **2012**, *24*, 6181−6185.
(48) Lan, X.; Voznyy, O.; Kiani, A.; García de Arquer, F. P.; Abbas, A. S.; Kim, G.-H.; Liu, M.; Yang, Z.; Walters, G.; Xu, J.; et al. Passivation Using Molecular Halides Increases Quantum Dot Solar Cell Performance. *Adv. Mater.* **2016**, *28*, 299−304.
(49) Allgaier, R. S.; Scanlon, W. W. Mobility of Electrons and Holes in PbS, PbSe, and PbTe between Room Temperature and 4.2 K. *Phys. Rev.* **1958**, *111*, 1029.
(50) Lee, S.; Zhitomirsky, D.; Grossman, J. C. Manipulating Electronic Energy Disorder in Colloidal Quantum Dot Solids for Enhanced Charge Carrier Transport. *Adv. Mater.* **2016**, *28*, n/a.
(51) Zhitomirsky, D.; Kramer, I. J.; Labelle, A. J.; Fischer, A.; Debnath, R.; Pan, J.; Bakr, O. M.; Sargent, E. H. Colloidal Quantum Dot Photovoltaics: the Effect of Polydispersity. *Nano Lett.* **2012**, *12*, 1007−1012.
(52) Hyun, B.-R.; Zhong, Y.-W.; Bartnik, A. C.; Sun, L.; Abruna, H. D.; Wise, F. W.; Goodreau, J. D.; Matthews, J. R.; Leslie, T. M.; Borrelli, N. F. Electron Injection from Colloidal PbS Quantum Dots into Titanium Dioxide Nanoparticles. *ACS Nano* **2008**, *2*, 2206−2212.

DOI: 10.1021/acs.chemmater.6b00167
Chem. Mater. 2016, 28, 1888−1896